University of Szeged

Graduate School of Pharmaceutical Sciences

Department of Pharmaceutical Technology

Ph.D. Thesis

Development and characterization of modified release oral preparations containing riboflavin

by

Gyula Buchholcz

Pharmacist

Supervisor:

Prof. Dr. Habil. Klára Pintye-Hódi Ph.D., D.Sc.

Szeged

2015

University of Szeged
Graduate School of Pharmaceutical Sciences

Educational Program: Pharmaceutical Technology
Head: Prof. Dr. Habil. Piroska Szabó-Révész Ph.D.,D.Sc.

Department of Pharmaceutical Technology
Supervisor: **Prof. Dr. Habil. Klára Pintye-Hódi Ph.D., D.Sc.**

Gyula Buchholcz

Development and characterization of modified release oral preparations containing riboflavin

Final Exam Committee:

Head: *Prof. Dr. István Erős*, University of Szeged, Dept. of Pharmaceutical Technology

Members: *Dr. Ildikó Bácskay*, University of Debrecen, Dept. of Pharmaceutical Technology
Dr. Gábor Blazsó, University of Szeged, Dept. of Pharmacodynamics and Biopharmacy

Reviewer Committee:

Head: *Prof. Dr. Mária Báthori*, University of Szeged, Dept. of Pharmacognosy

Reviewers: *Dr. István Antal*, Semmelweis University, Department of Pharmaceutics
Dr. János Bajdik, Meditop Ltd., Pilisborosjenő

Members: *Dr. Miklós Vecsernyés*, University of Debrecen, Dept. of Pharmaceutical Technology
Dr. Zsolt Szakonyi, University of Szeged, Institute of Pharmaceutical Chemistry

Szeged
2015

1 INTRODUCTION

The vitamins essential for living organisms are normally consumed in small amounts with the food. These organic materials facilitate the biochemical reactions that produce, among others, skin, bone and muscle. Once growth and development are completed, the vitamins remain essential nutrients for the healthy maintenance of the cells, tissues and organs; they also ensure the efficient use of the chemical energy provided by the food and promote the processing of the proteins, carbohydrates and fats required for respiration.

Riboflavin, a sparingly water-soluble vitamin that is a component of the co-enzymes flavin adenine dinucleotide (FAD) and flavin mononucleotide (FMN) is important in the utilization of food and the interconversion of energy.

Riboflavin has no overt pharmacological effects following its oral or parenteral administration. FMN and FAD, the physiologically active forms of riboflavin, serve a vital metabolic role as coenzymes for a wide variety of respiratory flavoproteins, some of which contain metals (e.g. xanthine oxidase). A deficiency of vitamin B_2 is associated with eye and skin disorders.

There are a number of preparations containing riboflavin on the market, e.g. effervescent tablets and instant granules. Modern therapy additionally requires a modified release dosage form since the riboflavin-containing drugs have poor oral bioavailability due to the narrow absorption window in the gastrointestinal tract.

2 AIMS

Riboflavin is readily absorbed from the upper gastrointestinal tract by a specific transport mechanism involving phosphorylation of the vitamin to FMN. Here and in other tissues, riboflavin is converted to FMN by flavokinase, in a reaction that is sensitive to the thyroid hormone status. Altough riboflavin is widely distributed in the body tissues, little is stored in the body.

Riboflavin may be absorbed in the duodenum and jejunum, but the extent of absorption at these sites is limited because the passage through this region is rapid. The bioavailability of riboflavin may be increased by the administration of a gastroretentive or modified release dosage form. Techniques are available that permit the production of drugs with poor colonic absorption, but better absorption properties in the upper parts of the gastrontestinal tract. These dosage forms may provide excellent results with drugs that act locally in the upper regions of the gastrontestinal tracts.

The main goal of the work reported in the thesis was to examine the possibility of improving

the bioavailability of narrow absorption window drugs through the use of film-coated capsules and modified release monolithic matrix tablets. The secondary goal was to identify relationships between the rate of release of the drug from capsules or tablets *in vitro* and the corresponding pharmacokinetic profile.

3 EXPERIMENTAL PART

3.1 SAMPLES I. Production of modified release capsules

3.1.1 Materials

Sodium riboflavin 5'-phosphate was used as active agent 1.0 g of sodium riboflavin 5'-phosphate is equivalent to about 0.73 g of riboflavin. This salt dissolves in water more easily than riboflavin itself, but it has the same absorption and excretion characteristics as those of riboflavin.

Cellet 300 served as core material and Eudragit NE 30D as coating material. The coating dispersion contained Dimeticon E and hydrophilic colloidal silicon dioxide and talc as anti-sticking agents. Ethanol 96% and purified water were used as solvents.

3.1.2 Methods

3.1.2.1 Core layering

The core pellets (Cellet 300) were loaded with a 10% aqueous solution of sodium riboflavin 5'-phosphate by a layering technique in a coating pan. The rate of rotation speed of the coating pan was 23 rpm. The nozzle size of the Walther spray gun was 0.8 mm. The atomizing spraying pressure was 0.6 bar and the spraying rate was 5 ml/min. The drying temperature was adjusted to 30-35 ºC.

The Cellet layered with sodium riboflavin 5'-phosphate was filled into hard HPMC capsules. A Zuma 150/A4 semiautomatic capsule filling machine was used.

3.1.2.2 Capsule coating

The composition of the coating dispersion was as follows:

Eudragit NE 30D 75.24 g, Dimeticon E 5.8 g, Aerosil 200 0.44 g, ethanol 96% 18.68 g, talc 3.34 g, and purified water 86.74 g. The nozzle size and type were the same as in the layering process. The atomizing spraying pressure was 0.8 bar and the spraing rate was 5 ml/min. The coating pan was rotated at 23 rpm, and the drying temperature was 25-30 ºC.

The coating dispersion was used in various quantities: 50.0 g (capsule A: dry material content: 7.5 g), 100.0 g (capsule B: dry material content: 15.0 g) or 250.0 g (capsule C: dry material content: 32.0 g).

3.1.2.3 Tests on coated capsules

Coating film thickness

A Mitutoyo screw micrometer was used to determine the thicknesses of the coating film on the cap and the corpus of the capsules. The diameter of the capsule was measured with 0.001 mm accuracy before and after coating.

Dissolution tests

The rate of dissolution of the drug was determined by the Münzel half-change method. This allows the use of artificial gastric fluid and artificial intestinal fluid of varying pH values in the range 1.2-7.5.

Dissolution tests were carried out in an Erweka DT 700 dissolution apparatus, using a paddle method. The volume of the dissolution medium was 900 ml. The test started with gastric fluid (without enzymes), and after each hour a sample was taken for concentration determination, and half of the bulk solution was then replaced with fresh intestinal fluid. The dissolution temperature was maintained at 37 ± 0.5 °C and the rotation rate was set at 100 rpm. Samples (5 ml) were collected automatically from the dissolution medium at 1, 2, 3, 4, 5, 6 and 7 h. Three replicates were tested for each capsule formulation batch. Absorbance was measured spectrophotometrically at λ_{max} = 266 nm. At any time (t), the total quantity of drug released from the capsule is defined.

3.1.2.4 Statistical evaluation

Model-independent evaluation

The dissolution efficiency (*DE*) can be calculated via the following expression:

$$DE = \frac{\int_0^t m(t)dt}{m_{100}t} \cdot 100 \qquad (1)$$

where *m(t)* is the amount of API dissolved at time *t*, and m_{100} is the amount of API dissolved at 100% dissolution.

Model-dependent evaluation of dissolution curves

Depending on the shape of the dissolution curve, various mathematical models can be used to describe the dissolution process (first-order, Higuchi, Hixson–Crowell, Hopfenberg, Korsmeyer–Peppas, Rosin–Rammler–Sperling–Benett–Weillbull (RRSBW) (modified Weibull), etc.). The RRSBW model is generally utilized to describe the dissolution profile in the event of a sigmoid shape. Another model that can be used in this case is the Chapman–Richards model.

The coefficient of determination (R^2) is frequently used as criterion to assess the best model equation. In this study we applied RRSBW distribution and the Chapman–Richards growth function to fit the dissolution profiles.

RRSBW model

RRSBW distribution is commonly used as the mathematical model in dissolution studies. This distribution is generally described by the following empirical equation:

$$M(t) = M_{\infty}(1 - e^{-\frac{(t-T)^{\beta}}{a}}) \quad (2)$$

where *M(t)* is the amount of API dissolved as a function of time *t*, M_{∞} is the maximum amount of API dissolved, *T* is the lag time, *a* is a scale parameter that describes the time dependence, and β describes the shape of the curve.

For $\beta = 1$, the shape of the curve corresponds exactly to the shape of an exponential profile with constant $k = 1/a$. This implies first-order kinetics in the dissolution process:

$$M(t) = M_{\infty}(1 - e^{-k(t-T)}) \quad (3)$$

For $\beta = 0$, the equation is

$$M(t) = M_{\infty}(1 - e^{-\frac{1}{a}}) \quad (4)$$

For $\beta < 1$, relatively rapid dissolution is observed at the beginning of the process, followed by a slower process.

For $(t-T)^{\beta} = a$, the equation is

$$\frac{M(t)}{M_{\infty}} = 1 - e^{-\frac{a}{a}} = 1 - e^{-1} = 0.632 \quad (5)$$

where $a = t_{63.2\%}$ is a characteristic dissolution time.

Chapman–Richards model

The Chapman–Richards method involves a 3-parameter sigmoid growth function based on the Bernoulli differential equation. This differential equation is used to describe the growth of an arbitrary quantity as the difference between its constructive growth and destructive growth:

$$\frac{dM}{dt} = \alpha M^{\beta} - \gamma M \quad (6)$$

where *M* is the quantity, αM^{β} is the constructive part and γM is the destructive part. The general solution of this differential equation is the 3-parameter Chapman–Richards function:

$$M(t) = M_{\infty}(1 - e^{-kt})^{\beta} \qquad (7)$$

where M_{∞}, k and β are the regression parameters to be estimated.

The dissolution profiles were fitted with Eq. 7, where *M(t)* is the amount of API dissolved as a function of time, M_{∞} is the total amount of the API, k is the dissolution rate and β describes the shape of the curve, which refers to the lag time of the dissolution.

As in the RRSBW model, $\beta = 1$ implies first-order kinetics.

3.1.3 Results

Coating film thickness

The film thickness the and uniformity of the coating play an important role in the dissolution. It was therefore important to determine the film thickness. The measurement data are summarized in Table 1.

Table 1. Film thickness on the capsule surface

Capsule	Film thickness (μm)	
	Cup	Corpus
A	161 ± 12	182 ± 5
B	200 ± 20	240 ± 36
C	227 ± 26	269 ± 36

The film thickness is seen to increase with increase of the coating dispersion, but the data also reveal a difference in the thickness of the films on the cup and the corpus of the coated capsules. The latter is primarily due to the shape of the capsules: there is always some difference (~30-40 μm) in the diameters of the cup and the corpus. The difference in the film thickness is not more than in the case of the uncoated capsule. This suggests that the coated dispersion spreads on the surface of the capsules during coating, and forms a uniform coating film on the surface of the capsules.

Dissolution tests

In the first step, we tested the rate of dissolution rate of riboflavin from uncoated capsules in artificial gastric fluid for comparison with the coated capsules. The results showed that the total riboflavin (100%) dissolved during 60 min.

The dissolution tests (by half change method) on the coated capsules clearly demonstrated the influence of the film thickness on the release of the drug (Fig. 1.).

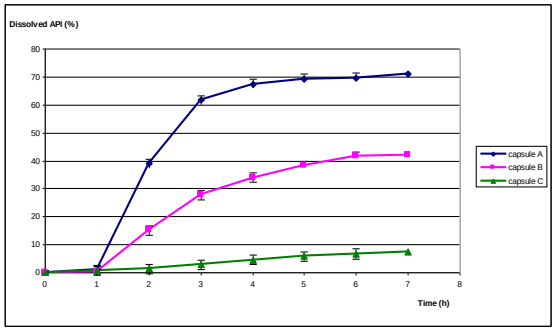

Figure 1. Dissolution of riboflavin from coated capsules

Table 2. Parameters of dissolution curves

Capsule	RRSBW model			Chapman–Richards model			
	β	a	R^2	M_∞	β	k	R^2
A	1.3602	1.3186	0.9171	69.6771	16.8461	1.66817	0.9991
B	1.6813	2.4113	0.9228	42.2965	5.2131	0.8363	0.9970

The dissolution profile exhibited a sigmoid shape in the cases of capsules A and B. These are typical dissolution curves of a delayed-release dosage form. However, capsule A is to be preferred in view of the present aim, because much of the API (~70%) was released at pH ≈ 7. The independent statistical evaluation of the results demonstrated that the efficiency of the mechanism of dissolution (*DE*) was highest in the case of capsule A.

Table 3. Results of the model-independent evaluations

Capsule	*DE* (%)
A	54.14
B	28.47
C	4.2

Various mathematical models were tested to describe the dissolution process (see above), and the RRSBW and Chapman–Richards model proved best. The results with these are presented in Table 2.

The R^2 data revealed that the dissolution curves for capsules A and B are well described by the Chapman–Richards equation.

The curve for capsule C was fitted by linear fitting (R^2= 0.9949), but the corresponding *DE* was not high enough, and hence it was not considered further.

The data in Table 3 demonstrate that the *DE* of capsule A was best, but the amount of API dissolved was only ≈70%. It is also evident that the coating film thickness influences the degree of dissolution of the drug. The question arises as to how the bioavailability of riboflavin

from the capsules can be enhanced. What is the best film thickness for total release to be attained in the small intestine during 2-5 h?

To answer this question, we created a theoretical model based on the Chapman–Richards method with respect to the fitting results. In this model, 95-100% of the API is released between 2 and 5 h. On the basis of this theoretical model and the measurement results, we calculated the optimum thickness of the coating via the following formula:

$$d_{opt} = d_A - (d_B - d_A)\frac{s_m - s_A}{s_A - s_B} \qquad (8)$$

where d_{opt} is the optimum thickness, d_A, and d_B are the thicknesses of the films on capsule A and capsule B, s_m is the slope of the model dissolution profile, and s_A and s_B are the slopes of the dissolution curves for capsule A and capsule B, respectively.

In this case, the predicted optimum film thickness on the corpus which ensures the required dissolution is 112.1 μm (Fig. 2.).

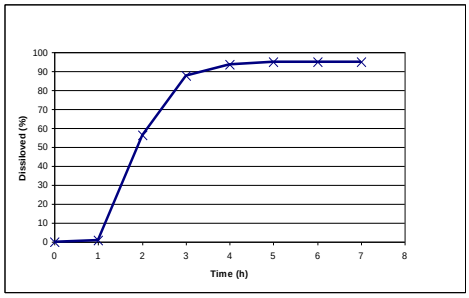

Figure 2. Predicted dissolution profile at a film thickness of 112.1 μm on the corpus

3.1.4 Discussion

In this work, a new solid dosage form was developed through the layering of aqueous sodium riboflavin 5'-phosphate solution on the surface of microcrystalline pellets (Cellet 300) as core material, which were then filled into capsules. The hard capsules were coated with Eudragit NE coating material in different thicknesses. Naturally, further pharmacokinetic testing is necessary to confirm the appropriate bioavailability. Statistical analysis of the dissolution curves indicated that the best products were described by the Chapman–Richards equation. The results were utilized to create a theoretical model suitable for prediction of the optimum

3.2 PRODUCTS II. Development of matrix tablets

3.2.1 Materials

Sodium riboflavin 5'-phosphate was used as API, Gelcarin GP 379 NF (iota-carrageenan) as swellable matrix material, microcrystalline cellulose (MCC) (Vivapur®

102) as non-swellable matrix-forming wicking material, and lactose as a filling excipient.

3.2.2 Methods

3.2.2.1 Preparation of granules

The homogenization and wetting of the powder mixture were performed in a high-shear mixer (ProCepT 4M8 granulator).

The ratios of the powder components were varied according to a 3^2 factorial design, as in Table 4.

Table 4. Compositions of powder mixtures

Gran code	**Iota-carrageenan (%)**	**MCC (%)**	**α-lactose monohydrate (%)**	**MCC/(MCC +lactose) ratio (%)**
Gran1	30	45	25	64.5
Gran2	30	55	15	78.6
Gran3	30	35	35	50

Homogenization parameters: impeller speed 1000 rpm, chopper speed 0 rpm, homogenization time 5 min

Kneading parameters: impeller speed: 1000 rpm, chopper speed 5000 rpm, dosing speed 10 ml/min, amount of API solution 120 ml (in three portions)

The wet granules obtained were sieved through a sieve with 1.2 mm wire distance and were dried at 22 ± 2 ºC/65 ± 5% relative humidity.

3.2.2.2 Tableting

The dry granules were mixed with 2% of magnesium stearate in a Turbula mixer at 50 rpm, for 2 min. The resulting granules were compressed into tablets at 5, 10 or 15 kN with a Korsch EK0 instrumented eccentric tablet machine. The compression tools were slightly concave punches 9 mm in diameter, the pressure force was calibrated with a Wazau HM-HN-30kN-D cell, and the compression was carried out electrically at 36 rpm, at 24 °C air temperature and 45% relative air humidity. The average mass of the tablets was 0.200 ± 0.01 g. 500 tablets were compressed at each compression force for each sample (when possible). Lots with relative standard deviations not exceeding 5% were accepted.

Model tablets *for swelling investigations* were also prepared with the above-mentioned Korsch EK0 eccentric tableting machine, but these tablets contained only the matrix former polymer (iota-carrageenan). The applied compression forces were again 5, 10 and 15 kN.

3.2.3 Physicochemical evaluation of tablets

The average and individual masses were measured with an analytical balance. The breaking strength, friability and geometry of the tablets, including thickness and diameter, were determined. 20 tablets were tested in every case.

3.2.4 Dissolution study and release modelling

Dissolution tests were carried out in an Erweka DT 700 dissolution apparatus, using the paddle method (Dissolution test for solid dosage forms – Apparatus 2 (paddle method).

The dissolution was tested in gastric fluid (pH = 1.2) and phosphate buffer (pH = 4.5). At the beginning of the process, the dissolution medium was 900 ml of gastric juice (adjusted according to the Ph. Eur.). The dissolution temperature was maintained at 37 ± 0.5 °C and the rotation rate was set at 100 rpm. Samples (2 ml) were automatically collected from the dissolution medium at 30, 60, 90 and 120 min. The dissolution medium was then changed to phosphate buffer under the former conditions and samples were again taken at 30, 60, 90, 120, 150 and 180 min. The total potential dissolution time was therefore 300 min (5 h). Three replicates were tested for each tablet formulation batch. Absorbance was measured spectrophotometrically at λ_{max} = 266 nm.

The dissolution data were calculated by statistical analysis and the release profiles were fitted with different models.

3.2.5 Factorial design

To reveal the relationships between composition, process parameters and tablet properties, the experiments were performed according to a 3^2 full factorial design (Statistica for Windows). The independent factors were the MCC/(MCC + lactose) ratio in the composition and the applied compression force. The optimization parameters were the amount of API dissolved after 5 h, and the friability and breaking hardness of the tablets.

3.2.6 Measurement of swelling

Swelling force was measured with equipment developed in our laboratory. Tablets were prepared at different pressures and their swelling was tested in hydrochloric acid of pH 1.2 and in phosphate buffer of pH 4.5. The temperature applied was 37 ºC and the duration of measurements was 30 min. Five parallels were measured.

The measurement was performed with a Sartorius microbalance with electronic compensation, built into the equipment with the DAQ hardware. The built-in DAQ unit is based on a PIC16F871-I/P microcontroller. The Sartorius balance and the temperature sensor were connected to ADC channel 0 and channel 1, respectively. The equipment was linked to a PC via an RS232 cable as shown in Fig. 3.

The tablet-holder was a copper cylinder 10 mm in diameter with slits in the side, into which a copper punch with the same diameter was fitted. The tablet was placed in the holder, the equipment heated the aqueous solution to the desired temperature, the liquid was injected and measurements were started.

The aqueous solution penetrated into the tablet through the slits. The force that built up inside the comprimate as it absorbed the liquid was transmitted vertically and was detected by the built-in Sartorius balance. During the measurement, the embedded software used the timer interrupt for the DAQ from the ADC channels.

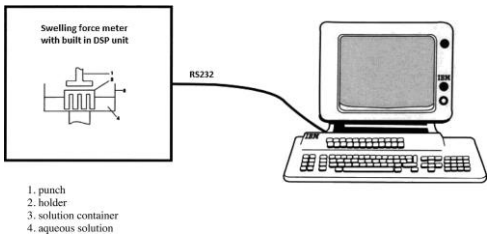

Figure 3. Experimental set-up of the swelling force meter

Software was developed for data acquisition, evaluation and demonstration of the swelling process. The monitor displayed the swelling force vs. time curve with the important parameters (the swelling force and the characteristic swelling time ($t_{63.2\%}$)). An Analysis menu facilitated fitting of the swelling curve.

3.2.7 Results and discussion

3.2.7.1 Granulation

It was clear there were not great differences in impeller torque, but there was a tendency for the end-point to increase to a small degree with increase of the lactose content. The impeller torque was 23% at the MCC/(MCC + lactose) ratio of 78.6% (*Gran2*); 26% at the MCC/(MCC + lactose) ratio of 64.5% (*Gran1*), and 31% at the MCC/(MCC+lactose) ratio of 50% (*Gran3*).

3.2.7.2 Tableting

The redispersed dry granules (moisture content: 5.00 ± 0.5%) were mixed with magnesium stearate and compressed. The physicochemical parameters of the tablets are presented in Table 5.

It can be seen from the data that the accuracy of the mass was good; this means that the flowability of the granules and the filling of the die cavity were uniform. The mechanical parameters (breaking hardness and friability) demonstrate the differences between the samples.

Table 5. Physicochemical parameters of tablets

Samples	**Compression force (kN)**	**Mass (g)**	**Breaking hardness (N)**	**Friability (%)**	**Diameter (mm)**	**Height (mm)**
Ribotab1 (ratio 64.5)	5	0.192	48.35	0.50	8.994	2.597
	10	0.211	50.90	0.48	8.999	2.526
	15	0.204	54.80	0.43	8.993	2.444
Ribotab2 (ratio 78.6)	5	0.195	37.50	1.54	8.911	2.409
	10	0.197	37.10	1.21	8.932	2.445
	15	0.195	37.60	1.07	8.940	2.421
Ribotab3 (ratio 50)	5	0.200	38.63	0.33	9.058	2.508
	10	0.210	57.95	0.36	9.036	2.507
	15	0.200	59.40	0.14	9.033	2.383

The results were evaluated according to the factorial design, the factors are described in section 3.2.5. The design matrix and the corresponding results are to be seen in Table 6.

Table 6. Design of experiments

MCC/(MCC + lactose) ratio (%)	Compression force (kN)	Breaking hardness (N)	Friability (%)	Amount of drug dissolved after 5 h (%)
50.0	5.0	38.63	0.33	100
50.0	10.0	57.95	0.36	100
50.0	15.0	59.40	0.13	82
64.5	5.0	48.35	0.50	65
64.5	10.0	50.90	0.48	63
64.5	15.0	54.80	0.42	51
78.6	5.0	37.50	1.54	71
78.6	10.0	37.10	1.22	84
78.6	15.0	37.60	1.07	82

The mechanical properties of the tablets seemed more robust than the dissolution data. (The dissolution curves are displayed below.) Neither the composition nor the compression force influenced this parameter significantly (Eq. 9); only the linear component of the MCC/(MCC + lactose) ratio proved to be of minor significance when the non-linear interactions were not taken into account, but this resulted in a decreased goodness of fit (R^2 = 0.8266 vs. 0.9393).

$$y = 46.91 - 7.30x_1 + 3.33x_1^2 + 4.55x_2 + 1.30x_2^2 - 5.17x_1x_2 - 2.35x_1x_2^2 - 1.23x_1^2x_2^2 \quad (9)$$

The decreasing value of the breaking hardness (Fig. 5.) and the corresponding increase in friability (Fig. 6.) may be due to the resistance of the granules against compression at high MCC content.

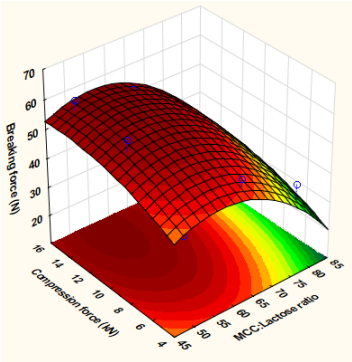

Figure 5. Response surface for the breaking hardness of the tablets

The results suggest that MCC loses its deformability during granulation, which results in a decreased binding capacity and a decreased mechanical strength of the tablets. Nevertheless, the mechanical problems are connected more with the abrasion than with the breaking of the tablets, as indicated by the higher sensitivity of the friability to the composition of the tablets (Eq. 10).

$$y = 0.67 + \mathbf{0.50}x_1 - \mathbf{0.15}x_1^2 - 0.12x_2 + 0.008x_2^2 - 0.07x_1x_2 \quad (10)$$

The significant factors are indicated with bold-faced type.

The MCC/(MCC + lactose) ratio significantly influenced the friability both linearly and non-linearly. Unfortunately, the consideration of the quadratic interactions resulted in overdetermination of the model, and these effects were therefore neglected during the analysis. The data in Table 4 demonstrate that in the case of *Ribotab1* [MCC/(MCC + lactose) ratio 64.5%] the compression force did not influence the hardness of the tablets or the geometrical parameters. The *Ribotab2* tablets exhibited a very a small breaking hardness, which was independent of the compression force. These tablets contained the smallest proportion of lactose (*Gran2*). With the MCC particles, the carrageenan formed a monolithic matrix with elastic behavior, which was not disturbed by the lactose particles. This was explained by the friability values, which revealed a higher elastic recovery in the tablets after compression. The compensatory behaviour of the MCC particles was not sufficient. *Ribotab3* was prepared with much more lactose (*Gran1*). In this case the tablets produced at 5 kN exhibited a small breaking hardness, which increased with increasing compression force, especially at 10 kN. Further increase of the compression force caused only a very small increase in hardness. The friability values indicated stronger binding in the texture of the tablets in the elastic recovery phase.

The results of the statistical evaluation revealed that even when the non-significant interactions between the factors were taken into account, the goodness of the fitted model increased significantly. In the case of the API dissolution, the adjusted R^2 was 0.7712 with no

interactions, 0.9490 with linear interactions, and 0.9972 with the application of the quadratic interactions too. It can be concluded that the API dissolution is mostly affected by the MCC/(MCC + lactose) ratio, and a strong non-linear relation can be observed between these two parameters (Fig. 7.). The compression force applied had a non-significant effect on this parameter, but it strongly interacted with the compositional parameter (Eq. 11).

$$y = 77.56 - \mathbf{7.50x_1 - 13.42x_1^2} - 3.50x_2 + 3.58x_2^2 + \mathbf{7.25x_1x_2} - 2.63x_1^2x_2 - 0.81x_1^2x_2^2 \qquad (11)$$

The significant values are highlighted in bold-type format. The highest values of dissolution were observed at high lactose content, which can be explained by the increasing porosity of the matrix due to the dissolution of the lactose. Nevertheless, the higher dissolution rate at low lactose proportions may be due to the weak effect of the MCC which results in a higher rate of water penetration into the matrix and forced dissolution of the drug from the internal pores of the system.

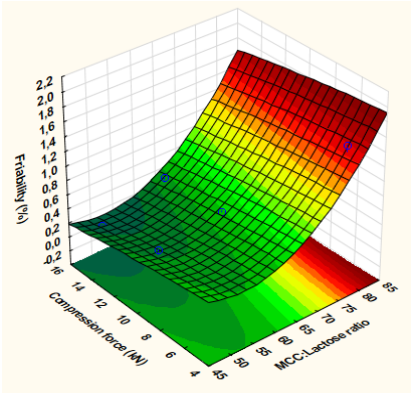

Figure 6. Response surface of the friability

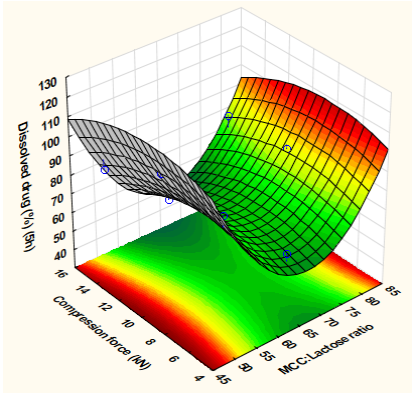

Figure 7. Response surface of drug dissolution

The dissolution curves of the tablets are displayed in Figs 8-10. It can be observed that the curves frequently display a break-point.

In the case of Fig. 8. *(Ribotab1)*, a break-point is not seen in the curve at 5 kN, but with increase of the compression force the break-point becomes clearer. This is in accordance with the hardness values of these tablets. In the tablets compressed at 5 kN, the binding can break more easily in the gastric juice; the texture of the tablets is more porous. The swelling of the macromolecular particles come off streamline; and at the change of the dissolution medium, the gastric juice can wash out readily from the matrix. In the case of a compact matrix system, it is more difficult for the phosphate buffer to pass into the interior of the tablet.

Ribotab2 (Fig. 9.) contained the lowest proportion of lactose. At 5 kN, where the matrix formed was more porous, the macromolecular particles could swell readily in the gastric juice and the API could dissolve. However the swelling later resulted in a gel form and, after the change of the dissolution medium, the phosphate buffer could not pass easily into the swollen particles; at first, a saturated section occurred in the dissolution profile. The degree of swelling of the carrageenan particles hindered the complete release of the API. In this case, the 10 kN compression force was best for the preparation of the tablets, because the texture of the tablets and the swellability were in equilibration. The release profile showed a uniform increase up to 80%. The tablets compressed at 15 kN also showed that the particles of the macromolecules did not swell to such a high degree and the dissolution rate was practically the same as for the former tablets.

Figure 10 best demonstrated the role of lactose during the dissolution process. The *Ribotab3* tablets contained lactose in highest proportion in the matrix system. The particles of lactose could disperse to a high degree between the macromolecular particles. It can be seen from Table 6 that the mechanical hardness of these tablets was the weakest; it is well known that lactose is a brittle material and is not able to form hard binding during loading. The dissolution process of the tablets compressed at 5 kN is not depicted here as the deviation was too high. Only the dissolution profiles, of the 10 and 15 kN tablets are illustrated. Lactose, a well-soluble excipient, which can be incorporated between the macromolecular particles, promotes the release of the API. The total amount of the API was dissolved from the tablets compressed.at 10 kN. Further increase of the compression force would not have been advantageous, because the more compact texture prevented the total dissolution of the API during 5 h.

The dissolution data were subjected to statistical analysis. The *Korsmeyer–Peppas model* (Eq. 12) proved to characterize the total dissolution profile best:

$$\frac{m_t}{m_\infty} = kt^n \qquad (12)$$

where m_t/m_∞ is the fraction of the API released at time t, k is the rate constant and n is the release exponent.

The R^2 values revealed rather strong correlations (Table 7.), but because of the break-points in the dissolution profiles, we took the dissolution data in two groups and fitted all the sections according to the Korsmeyer–Peppas and the linear model. The first section was the period 0-120 min and the other 150-300 min. The results are presented in Tables 8 and 9.

It can be seen from the data in Table 8 that the correlation is strong, especially in the first section of the dissolution profile.

The fitting with the *linear model* was also examined:

$$\frac{m_t}{m_\infty} = at + b \qquad (13)$$

where m_t/m_∞ is the fraction of the API released at time t, a is the slope and b is the intersection.

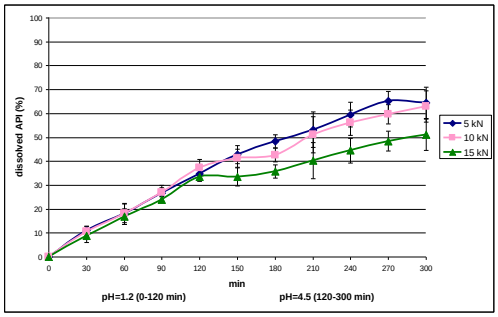

Figure 8. Dissolution curves for *Ribotab1* samples

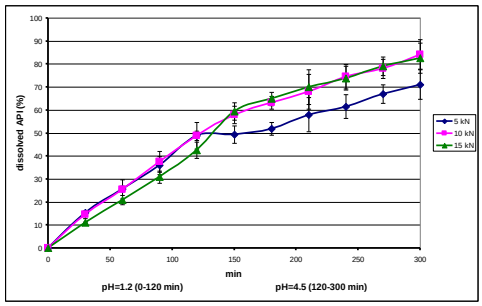

Figure 9. Dissolution curves for *Ribotab2* samples

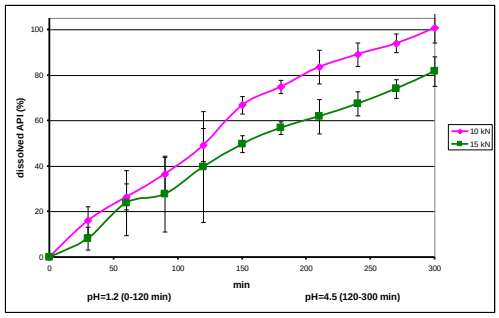

Figure 10. Dissolution curves for *Ribotab3* samples

The tablets produced at 5 kN exhibited a low breaking hardness, and the dissolution process was depicted here as the deviation was too high; these samples were omitted from the further experiments

Table 7. Fitting results of total dissolution profile

Samples	*k*	*n*	R^2
Ribotab1-5kN	0.9403	0.7525	0.9924
Ribotab1-10kN	1.0956	0.7149	0.9916
Ribotab1-15kN	1.2816	0.6483	0.9866
Ribotab2-5kN	2.6359	0.5789	0.9860
Ribotab2-10kN	1.7948	0.6788	0.9920
Ribotab2-15kN	1.0872	0.7700	0.9777
Ribotab3-10kN	1.2199	0.7808	0.9888
Ribotab3-15kN	0.7881	0.8148	0.9930

.

Table 8. Fitting results of each section of dissolution according to the Korsmeyer–Peppas model

Samples	0–120 min			150–300 min		
	k	*n*	R^2	*k*	*n*	R^2
Ribotab1-5kN	0.5277	0.8734	0.9986	1.8832	0.6262	0.9637
Ribotab1-10kN	0.3537	0.9690	0.9972	1.4535	0.6627	0.9705
Ribotab1-15kN	0.3052	0.9782	0.9982	1.2273	0.6547	0.9914
Ribotab2-5kN	0.7368	0.8723	0.9971	2.9937	0.5542	0.9870
Ribotab2-10kN	0.6548	0.9001	0.9996	3.7644	0.5434	0.9944
Ribotab2-15kN	0.3487	1.0011	0.9991	5.5042	0.4751	0.9987
Ribotab3-10kN	0.8557	0.8426	0.9971	3.7482	0.5771	0.9947
Ribotab3-15kN	0.4046	0.9562	0.9782	1.4330	0.7060	0.9929

Table 9. Fitting results of each section of dissolution according to the linear model

Samples	0–120 min			150–300 min		
	a	*b*	R^2	*a*	*b*	R^2
Ribotab1-5kN	0.2845	1.0700	0.9956	0.1574	20.1773	0.9545
Ribotab1-10kN	0.3025	0.4147	0.9972	0.1562	17.1817	0.9685
Ribotab1-15kN	0.2736	0.2423	0.9982	0.1246	14.2783	0.9929
Ribotab2-5kN	0.3946	1.5450	0.9943	0.1497	26.1577	0.9923
Ribotab2-10kN	0.4027	1.1415	0.9977	0.1742	31.7570	0.9961
Ribotab2-15kN	0.3494	0.1023	0.9991	0.1543	36.9603	0.9964
Ribotab3-10kN	0.3968	1.8949	0.9925	0.2213	35.0401	0.9890
Ribotab3-15kN	0.3300	0.1267	0.9776	0.2065	18.7888	0.9959

The results show, that both of the sections can be fitted by the linear model too. However the results with the Korsmeyer–Peppas model indicated that the matrix model fitting was better in most cases.

In earlier work, in which the swelling properties and swelling forces of different disintegrants were tested, it was concluded that in the case of disintegrating tablets the swelling curve can be fitted by the RRSBW equation (Eq. 2), and the swelling process can be characterized by the RRSBW model.

In the present work, we studied the swelling properties of matrix tablets. Gelcarin GP 379, a swellable carrageenan, was used in the present experiment, and the tablets did not contain other

excipients. The measured swelling force was therefore attributable only to the swelling of iota-carrageenan. The experiments were carried out at pH 1.2 and pH 4.5, both of which are to be found in the gastrointestinal tract. The results are shown in Table 10.

Table 10. Swelling of iota-carrageenan tablets

Compression force (kN)	pH	Swelling force (N)	Swelling time (min)
5	1.2	3.006 SD = ±0.098	28.54 SD = ±3.26
	4.5	2.952 SD = ±0.388	24.8 SD = ± 3.93
10	1.2	2.106 SD = ± 0.885	28.16 SD = ± 2.05
	4.5	3.19 SD = ± 0.316	27.58 SD = ± 2.89
15	1.2	2.364 SD = ± 0.78	28.52 SD = ± 2.88
	4.5	2.946 SD = ± 0.188	27.12 SD = ± 2.66

Duration of experiments: 30 min, temperature: 37 ± 1 ºC

The measured swelling force exhibited values only in the range 2-3 N, independently of pH and pressure, while the swelling time corresponding to the maximum swelling force was 25-28 min.

At the beginning of the process, fast swelling occurred, which was followed by slower swelling, but the force increased steadily. The curve could be fitted by the Korsmeyer–Peppas equation (r^2 = 0.9930) (Fig. 11.) from 0 min up to approximately 25-28 min. In the period of formation of the gel barrier, there is strong physicochemical bonding between the polymer particles. After this period, further water molecules penetrate into the matrix and rearrangement of the bonding between the polymers occurs. Our experiments demonstrated that from this point the curve is basically linear (Fig. 11.).

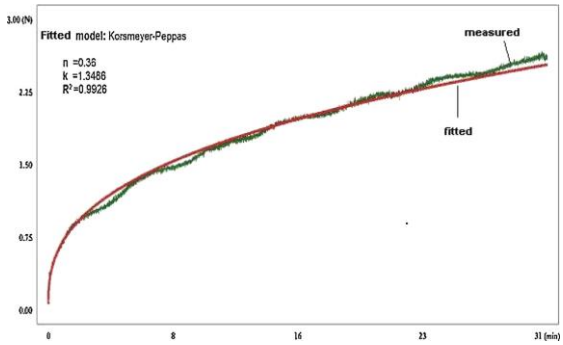

Figure 11. Swelling curve of iota-carrageenan comprimate (compression force: 15 kN).

The results demonstrated that the shapes of the swelling curves were independent of pH and the compression force. It may therefore be supposed that iota-carrageenan matrix tablets will

behave similarly in the gastrointestinal tract as concerns the process of dissolution from sustained-release tablets.

3.2.8 Conclusions

It was concluded that the lactose content influences the physical parameters, the degree of dissolution and the profile of dissolution. When the proportion of lactose was smaller, the elasticity of the matrix was higher, which resulted in tablets with weak mechanical properties. Furthermore, the macromolecular particles could swell very well in the dissolution medium. The dissolution profiles could be fitted best with the Korsmeyer–Peppas model, but thanks to the lactose content the dissolution sometimes occurred in two phases.

Application of a swelling force meter revealed the changes in the swelling force in matrix tablets. Two sections were observed in the swelling process: in the first, the degree of swelling and the swelling force were higher because of the strong bonds between the macromolecules, and this section could be fitted with the Korsmeyer–Peppas equation. In the second section, the bonds became weaker and the rate of increase of the swelling force decreased. This test characterized very well the swelling process of the matrix system.

4 FINAL CONCLUSIONS, NOVELTY, PRACTICAL USEFULNESS

As described in the Introduction the aim was to develop modified release preparations containing riboflavin by different technological methods. Riboflavin was particularly suitable because it is absorbed to only a limited extent in the duodenum and jejunum as its passage through this region is rapid. The bioavailability of riboflavin may be increased by administration of a gastroretentive or modified release dosage form.

The important novelty and practical usefulness of this work may be summarized as follows:

- A new solid dosage form was developed through the layering of aqueous sodium riboflavin 5’-phosphate solution onto the surface of microcrystalline pellets (Cellet 300 as core material), which were then filled into capsules.
- The coating of the capsules was investigated and the influence of the thickness of the coating layer on the dissolution of sodium riboflavin 5’-phosphate was tested. The optimum film thickness was predicted with regard to the modified release of sodium riboflavin 5’-phosphate.

- Monolithic matrix tablets containing sodium riboflavin 5'-phosphate were prepared by wet granulation according to a 3^2 full factorial design. A suitable MCC/lactose ratio and the best compression force were determined as concern an appropriate dissolution profile.
- A new swelling force meter was developed for measurement of the swelling force in matrix tablets and characterization of the profile of the swelling curve. The swelling force meter was linked to a PC by an RS232 cable and the measured data were evaluated with self-developed software. The monitor displayed the swelling force vs. time curve with the important parameters, which could be fitted with an Analysis menu. This equipment can be generally applied for matrix systems.

The results and observations of the present study provide useful information for industrial technologists.

PUBLICATIONS:

I. **Buchholcz Gyula**, Erős István, Hódi Klára:

Gyógyszer-filmbevonó anyagok és eljárások Fókuszban az Eudragit®.
Gyógyszerészet, 48, pp. 651-658 (2004)

II. **Buchholcz Gyula**, Hódi Klára:

Amit a vitaminokról röviden tudni kell – A sokoldalú B2-vitaminról bővebben.
Gyógyszerészet, 55, pp. 538-542 (2011)

III. **Gyula Buchholcz**, András Kelemen, Klára Pintye-Hódi:

Modified-release capsules containing sodium riboflavin 5'-phosphate.
Drug Development and Industrial Pharmacy, 2014, 40, 1632-1636 IF: 2.101

IV. **Gyula Buchholcz**, András Kelemen, Tamás Sovány, Klára Pintye-Hódi:

Matrix tablets based on a carrageenan with the modified-release of sodium riboflavin 5'-phosphate.
Pharmaceutical Development and Technology, 2014, DOI: 10.3109/10837450.2014.910810 IF: 1.202

V. András Kelemen, **Gyula Buchholcz**, Tamás Sovány, Klára Pintye-Hódi:

Evaluation of the swelling behaviour of iota-carrageenan in monolithic matrix tablets**.**
Journal of Pharmaceutical and Biomedical Analysis, 2015, 112, 85-88
IF: 2.979

PRESENTATIONS:

I. **Gy. Buchholcz**, I. Erős, J. Pintye, K. Pintye-Hódi: Preparation of sustained-release capsule containing sodium riboflavin phosphate pellets,
EAHP Congress Sevilla (2004)

II. **Buchholcz Gyula**, Erős István, Hódi Klára: B2-vitamin tartalmú kapszula előállítása,
MGYT KGYSZ Kongresszus Debrecen (2004)

III. **Gy. Buchholcz**, I. Erős, K. Pintye-Hódi: Influence of the thickness of coating films on the dissolution of sodium riboflavin phosphate,
CESPT Congress Siófok (2005)

IV. **Buchholcz Gyula**, Kelemen András, Sovány Tamás, Hódi Klára: Módosított hatóanyagleadású B2-vitamin tartalmú monolitikus mátrix tabletta előállítása,
Congressus Pharmaceuticus Hungaricus XV. Budapest (2014)